

Modified subband ARCAP method for the monitoring of rail corrugation

C. Hory, L. Bouillaut and P. Aknin

LTN-INRETS

2, rue de la Butte Verte, 93166 Noisy-le-Grand Cedex

(ph) +33 (0)1 45 92 56 49

(f) +33 (0)1 45 92 55 01

hory@inrets.fr

S. Bondeux

VOIE-EST-RATP

50, rue Roger Salengro, 94724 Fontenay-sous-Bois Cedex

Abstract

Rail corrugation is an undulatory mechanical wear of rail surface raising from the interaction between rail and wheel. Signal processing approaches to corrugation monitoring recommended by the European standards are designed in the distance or wavelength domain. However a joint distance and wavelength domain analysis of the monitoring data can provide crucial information about the distance-evolution of the corrugation modes. We have recently proposed to perform such a distance-wavelength domain analysis using the ARCAP method. This method assumes a model of the data that fits well to a sum of sinusoids. Since each corrugation mode is described by a sinusoid, the ARCAP method is a good candidate for corrugation analysis. Experimental studies performed on data collected on the French RATP metro network have shown that the ARCAP method outperforms the standard distance or wavelength domain methods in localizing and characterizing corrugation. However the ARCAP method suffers from two drawbacks: the amplitude estimator is known to be biased and a priori knowledge of the number of corrugation modes is required. In this contribution we explore a modification of the ARCAP method aimed at tackling these drawbacks. We propose to estimate the corrugation depth using the unbiased APES technique in order to get a more reliable estimation of the amplitude and phase of the modes. We propose also to incorporate a sub-band spectral estimation step so that to improve the frequency estimation performance of the method.

1. Introduction

Rail corrugation ^(1,2) is a vibrational wear phenomenon occurring on some railway transportation systems and mostly in urban areas. It is a consequence of the mechanical interaction between the passing train and the rail depending mainly on the oscillating characteristics of the train and on the mechanical properties of the rail and wheels. Rail

corrugation can be considered as a closed loop combination of a wavelength fixing mechanism and a damage mechanism ^(2,3). The consequence is an oscillatory vertical wear of the rail along the longitudinal axis as observed on Figure 1.

Rail corrugation is a source of noise and vibration for the surrounding neighbourhood and passengers. It reduces the lifetime of both wheels and rails but also of other components of tracks and boggy. For environmental as well as economical issues, reducing - if not annihilating - rail corrugation is thus a matter of great concern for railway networks.

Many studies have been dedicated to the comprehension of the rail corrugation phenomenon ⁽²⁻⁴⁾. Even though chemistry, matter physics and mechanics can help devising new railtrack materials with a longer lifetime, it is almost impossible to avoid rail corrugation. Diagnosis have thus to be performed on existing railway network so that to detect and cure rail corrugation following a determined maintenance strategy.



Figure 1. Corrugation on the line A of the Paris RER network between Fontenay-aux-Roses and Robinson stations.

Techniques based on the European standard recommendations ⁽⁵⁾ for corrugation monitoring consists in setting a threshold on the root-mean square of the band-pass filtered corrugation recording. Alternatively, it is proposed in the European standard ⁽⁶⁾ to threshold the Welch periodogram of the corrugation data. Either approaches to corrugation monitoring fail in providing information on the evolution of a given corrugation mode along mileage.

Time-frequency methods ⁽⁷⁾ are designed for the analysis of one-dimensional data in a joint time (or mileage) and frequency (or wavelength) domains. Caprioli et al ⁽⁸⁾ have recently proposed a comparative study of the application of two time-frequency tools to

the characterization of corrugation. However these two approaches, namely the spectrogram and the scalogram, give access to an estimation of the spectral power of the signal. Same remark holds for the periodogram mentioned by the European standard. Moreover the spectral resolution of these approaches is poor.

We propose in this paper to apply a time-frequency analysis tool introduced by Padovese et al called the ARCAP method ⁽⁹⁾. This method takes advantage of both the AR frequency estimation method ⁽¹⁰⁾ and the Capon approach ⁽¹¹⁾ in a joint formulation. The AR and Capon methods offer better resolution capabilities and better estimation performances than the spectrogram or scalogram. In addition the ARCAP method allows to estimate the depth of corrugation which leads to a straightforward interpretation for further diagnosis as opposed to spectral power density estimation.

However the amplitude spectral Capon estimator is known to be biased ⁽¹²⁾. We propose to replace the Capon method by the recently introduced APES ⁽¹³⁾ method which is unbiased ⁽¹²⁾. In addition AR spectral modelling has been shown to be more efficient in a filterbank approach ⁽¹⁴⁻¹⁵⁾. Since the Capon and APES are based on the design of a filterbank, we propose to combine these two approaches so that to improve the frequency estimation performance.

2. Diagnosis of rail corrugation

In this section the measurement set-up in use at RATP is briefly described and the deduced signal model is introduced.

2.1 Measurement set-up

The measurement device currently in use for corrugated rail inspection and corrugation diagnosis on the RATP network was described in a technical report ⁽¹⁶⁾. A picture and a schematic representation of the device are shown on Figure 2.

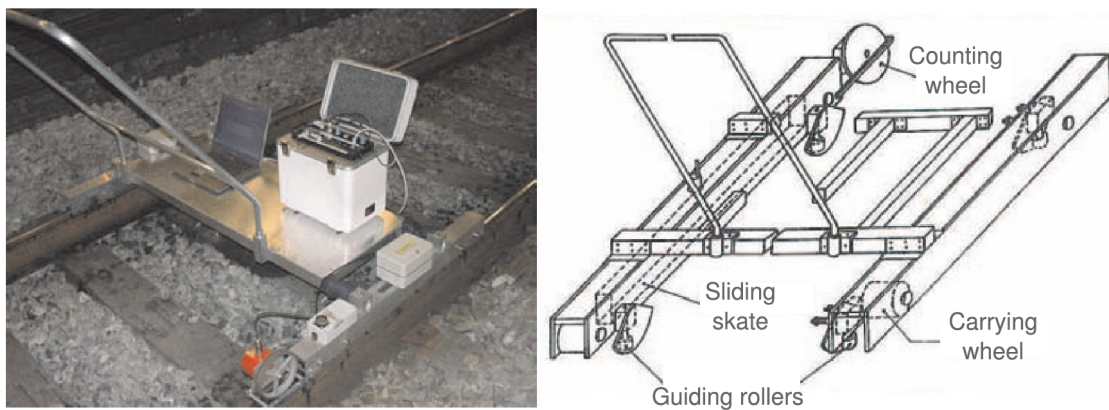


Figure 2: Measurement device. Courtesy of RATP.

An Eddy current sensor is fixed on a 80cm long sliding skate. The data acquisition system is carried on a trolley. The trolley is manually moved at human walking speed so

that the skate slides along inspected rail. The distance of the rail to the middle of the pad is measured every 2mm and recorded on the embedded computer.

2.2 Signal model

The measurement signal is filtered with a high-pass Butterworth filter of order 4 in order to remove the dynamic of the measurement device. The cut-off wavelength is of 1m. The signal is filtered twice (forward and backward) in order to avoid phase decay. The output sequence $x[k]$, for $k=1, \dots, N_x$, from which the corrugation diagnosis is to be performed is a sequence of N_x samples indexed by the mileage point index k . Assume a corrugation waveform encoded in the pre-processed signal can be approximated by a sinusoid. Each corrugation mode is thus characterized by its amplitude and natural frequency. Under a signal processing framework the corrugation task is then to detect and characterize sinusoids in noise. The characterization task consists in estimating the amplitude and natural frequency of the corrugation mode. Consider the complex signal $x[k]$ bearing I corrugation modes:

$$x[k] = \sum_{i=1}^I A_i[k] \exp(j\omega_i[k]k) + b[k], k=1, \dots, N_x, \quad (1)$$

where $A_i = \alpha_i[k] \exp(j\varphi_i)$ and $\omega_i[k]$ are respectively the complex amplitude and the natural frequency of the i th corrugation mode, and $b[k]$ is a white Gaussian noise with variance σ^2 . The diagnosis task consists in detecting the I corrugation modes and estimating the amplitudes $\alpha_i[k]$, and natural frequencies $\omega_i[k]$.

3. The ARCAP Method

The parameters of interest in the signal model (1) vary with the mileage index k . Time-frequency approaches⁽⁷⁾ are devoted to the analysis of such non-stationarities. The ARCAP method⁽⁹⁾ is a time-frequency signal processing method that jointly takes advantage of the good estimation performance of the Auto-Regressive (AR) spectral analysis approach⁽¹⁰⁾ and the Capon filter⁽¹¹⁾ (CAP).

A flowchart of the method is presented on Figure 3. Consider the N sample long signal segment $x^{[n]} = [x[n], x[n+1], \dots, x[n+N-1]]^T$ where \cdot^T denotes the transpose operation. From segment $x^{[n]}$, the ARCAP method first computes the AR estimates

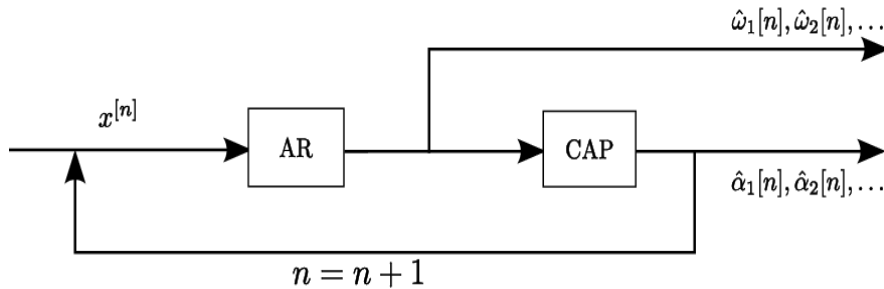


Figure 3: Flowchart of the ARCAP method.

$\hat{\omega}_i[n]$ of ω_i and then compute the Capon estimates $\hat{\alpha}_i[n]$ of α_i . The procedure is repeated for $n=n+1$, until $n=M=N_x-N+1$. The output is a mapping:

$$\mathbb{N} \cap [1 M] \rightarrow ((0, \pi) \times \mathbb{C})^q$$

$$n \rightarrow (\hat{\omega}_i[n], \hat{\alpha}_i[n]), i=1, \dots, q,$$

where $q \leq p$ is the number of estimated natural frequencies $\hat{\omega}_i \in (0, \pi)$. The AR and Capon steps are described in sections 3.1 and 3.2.

3.1 AR step: frequency estimation

Unless equivocal the segment index $[n]$ is omitted in the remaining of this paper. The AR spectral estimation techniques assume an order p AR – denoted AR(p) – modelling of the analysed data:

$$x[k] = -\sum_{l=1}^p a_l x[k-l] + \epsilon[k], \quad (2)$$

where $\epsilon[k]$ is a white Gaussian noise with variance σ_ϵ^2 called the innovation process and $a = [a_1, a_2, \dots, a_p]^T$ is the $p \times 1$ vector of AR coefficients. The AR(p) process is the output of an all-pole linear time-invariant system fed with the innovation process. The spectrum $X_{ar}(\omega)$ of the AR(p) process is thus ⁽¹⁷⁾:

$$X_{ar}(\omega) = \frac{\sigma_\epsilon^2}{|1 + \sum_{l=1}^p a_l \exp(-j\omega l)|^2}. \quad (3)$$

The AR spectral estimation approach consists in computing an estimate \hat{a} of a and injecting \hat{a} in (3). It is a parametric method and because of the a priori information encoded in the underlying modelling it is a *high-resolution* method provided the model fits the data.

Since estimation of the whole spectrum is unnecessary for the corrugation diagnosis task, it is more relevant and less time-consuming to estimate only the resonance frequencies of the system. Such estimators are provided by the angle of the roots of the polynomial:

$$A(l) = 1 + \sum_{l=1}^p \hat{a}_l z^{-l}.$$

The ARCAP method performs the AR-step using the modified covariance method ⁽¹⁰⁾. It is based on a least-square estimation of the AR coefficient vector involving the $p \times p$ forward-backward sample covariance matrix R_x of the data sample.

Once the frequencies have been estimated the second step of the method consists in estimating the corresponding amplitudes.

3.2 Capon step: Amplitude estimation

The Capon method ⁽¹¹⁾ was introduced in 1969 as a *high-resolution* power spectrum estimation technique in the sense that for an equivalent signal length it exhibits a lower spectral bandwidth than the Fourier methods. It has been shown more recently by Stoica et al. that the Capon method belongs to the family of matched-filter bank approaches ⁽¹⁸⁾. The Capon estimator is computed by designing a bank of filters that pass undistorted the analysed signal at the centre frequencies (gain unity) while minimizing the output power outside the filter band. This is a quadratic optimization problem. The Lagrange multiplier solution to this problem is the p sample long impulse response $h(\omega)$ of the filter with centre frequency ω :

$$h(\omega) = \frac{R_x^{-1} e(\omega)}{e(\omega)^H R_x^{-1} e(\omega)}, \quad (4)$$

where $e(\omega) = [1, \exp(j\omega), \dots, \exp(j(p-1)\omega)]$ and H stands for the complex conjugate transpose operation. Note that any N sample long signal can be written $x[k] = \alpha(\omega) \exp(i\omega k) + b_\omega[k]$. The least-square estimation $\hat{\alpha}(\omega)$ of $\alpha(\omega)$ is ⁽¹²⁾:

$$\hat{\alpha}(\omega) = h(\omega)^H X(\omega), \quad (5)$$

where $X(\omega) = \sum_{k=1}^{M-p+1} [x[k], x[k+1], \dots, x[k+p-1]]^T \exp(-j\omega k) / (M-p+1)$, is the Fourier transform of the analysed sequence.

Within the ARCAP framework the Capon amplitude estimator (5) is computed at those frequencies $\omega = \hat{\omega}_i$ estimated during the AR step. The ARCAP amplitude estimators are $\hat{\alpha}_i = \hat{\alpha}(\hat{\omega}_i)$. The resulting ARCAP map provides a representation of the analysed signal as sequences of couples $(\hat{\alpha}_i[n], \hat{\omega}_i[n])$, that characterize each individual corrugation mode. Because of the resolution capability, not only the ARCAP method allows for a better discrimination of the modes but it also provides a separated analysis of these modes for further interpretation.

4. Modifications of the ARCAP method

The ARCAP method was proposed in 1992 ⁽⁹⁾. Since then new theoretical results have been obtained which suggest some improvements of the method. In section 4.1 and 4.2 we propose two modifications of the ARCAP method aiming at increasing the performances of the estimators.

4.1 Improving the amplitude estimation with APES

In 1998 the Capon amplitude estimator was shown to be biased downwards ⁽¹²⁾. In this paper the Capon method was compared with other methods. Among others, the

Amplitude and Phase Estimator of Sinusoid (APES) introduced by Li and Stoica ⁽¹³⁾ was shown to be unbiased.

The APES method belongs also to the MAFI class ⁽¹⁸⁾. The expression of the impulse response is obtained from (4) by replacing the sample covariance matrix R_x by

$Q_x = R_x - X(\omega)^H X(\omega)$ where $X(\omega)$ is the Fourier transform defined in section 3.2:

$$h(\omega) = \frac{Q_x^{-1} e(\omega)}{e(\omega)^H Q_x^{-1} e(\omega)}. \quad (6)$$

Under the model $x[k] = \alpha(\omega) \exp(i\omega k) + b_\omega[k]$, mentioned in section 3.2, Q_x is an estimate of the noise covariance matrix. It can be shown that under this model the estimation $\hat{\alpha}(\omega) = h(\omega)^H X(\omega)$, obtained with the APES method is an approximate likelihood estimation of $\alpha(\omega)$. ⁽¹³⁾

4.2 Filterbank implementation

Since the APES method exhibits narrow spectral peaks, the amplitude estimation vanishes quickly with frequency. A small deviation of the frequency AR estimation can thus lead to a dramatic underestimation of the amplitude of the real frequency. The ARCAP and APES methods can be improved by improving the performance of the AR estimation.

The main drawback of AR spectral estimation is the risk of inadequacy of the model to the data. In particular a wrong estimation of the order of the model can dramatically decrease the accuracy of the estimation. Rao and Pearlman have shown that performing AR spectral estimation on a subband decomposition of the data allows to overcome this drawback ⁽¹⁴⁾. Tkacenko and Vaidyanathan have confirmed this result in the case of sinusoid frequency estimation ⁽¹⁵⁾.

A flowchart of the proposed modification of the ARCAP method is displayed on Figure 4. The Capon and APES methods implicitly compute the set of impulse responses of a bank of filters. We propose to filter the analysed segment $x^{[n+1]}$ with the $q^{[n]}$ Capon filters computed during the previous iteration of the algorithm.

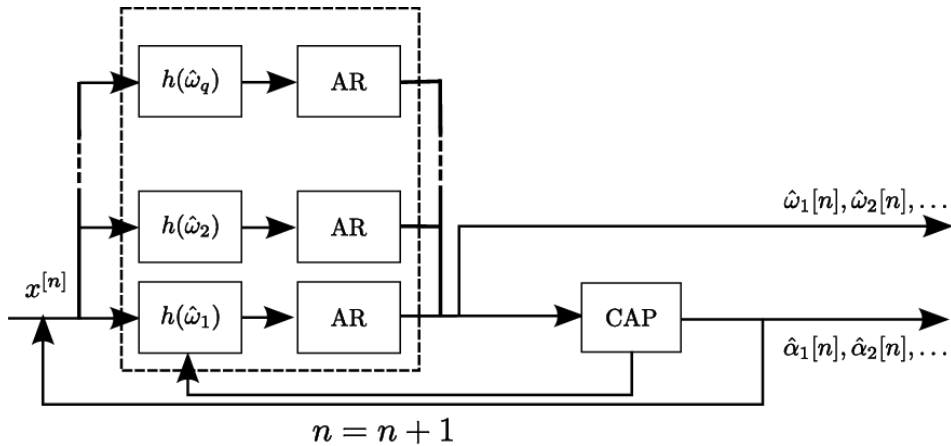


Figure 4: Flowchart of the filterbank implementation.

This filterbank implementation should allow for a gain in frequency estimation performance if the centre frequency of the i th filter is the frequency of interest $\hat{\omega}_i[n]$. We have experimentally observed that this assumption does not necessarily hold true. We have generated a $N_x=1000$ sample-long sum of two sinusoids embedded in a white Gaussian noise. The normalized natural frequencies of the modes are $\omega_1=2\pi 0.15$, and $\omega_2=2\pi \cdot f \cdot$. The respective amplitudes are $\alpha_1=1$, and $\alpha_2=2$, and the noise variance is $\sigma^2=1$, so that the local signal-to noise ratios defined as $snr_i=10\log(\alpha_i^2/\sigma^2)$, are $snr_1 \approx 0\text{dB}$ and $snr_2 \approx 6\text{dB}$. The Capon and APES methods were applied to the successive $N=50$ sample long segment of signal. The filter length was of $p=20$ samples. On Figure 5 are plotted in black the average gain of the $M=N_x-N+1=951$ computed filters for the frequency of interest ω_1 .

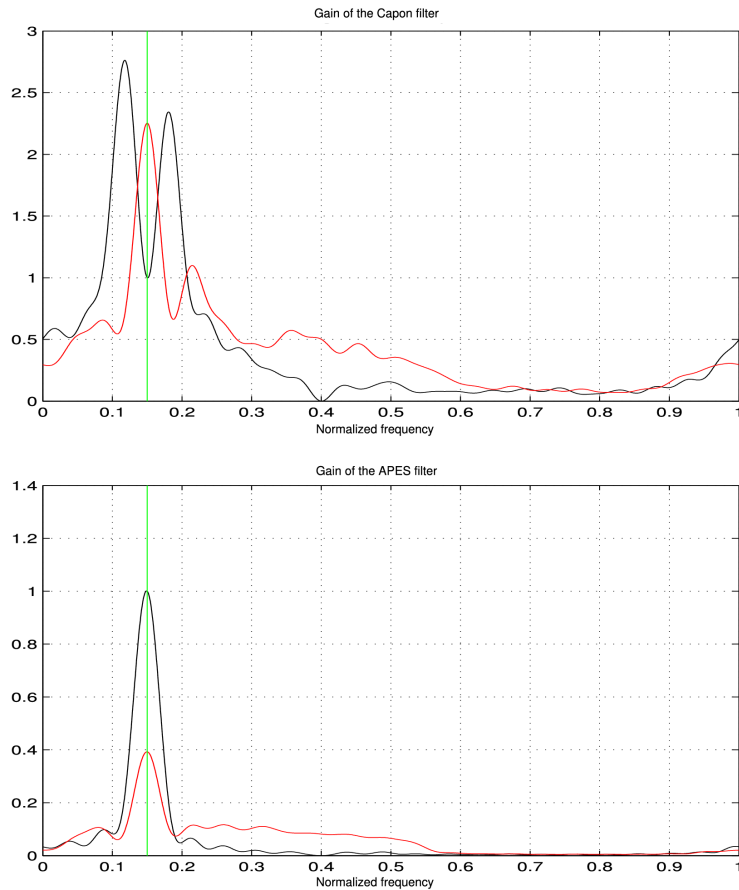


Figure 5: Average gain of the Capon (up) and APES (bottom) filters before frequency shift (black line) and after frequency shift (red line). Centre frequency: $\omega_c = 2\pi 0.15$ (green line) and local SNR 0dB.

As expected, both the Capon and APES filter gain is equal to unity at the frequency of interest. However one can observe that this optimization constraint does not impose the filter to be centred on the frequency of interest spotted with a green line. In the case of the Capon filter one can observe two shifted lobes around ω_1 .

Note that Durnerin et al pointed out the possible presence of two main lobes of the Capon filter gain at low local signal to noise ratio when the frequency of interest is close (but not equal) to the actual signal frequency ⁽¹⁹⁾.

On can conclude that the resulting filtered signal can be shifted in frequency which can lead to a decrease of the frequency estimation performance.

In order to overcome this problem the frequency of the main lobe of each impulse response has been estimated using the modified covariance AR(10) method. The estimated frequency has been used to shift the impulse response. The resulting average shifted gains are plotted in red on Figure 5.

The main lobes are centred on the frequency of interest. However there are still some side lobes. The Capon and APES filters are thus not band-limited.

5. Experimentation

We have performed 500 Monte-Carlo runs of the different method described in section 3 and 4 applied to the synthetic signal of Figure 5. The results are displayed in Table 1 in terms of relative bias and variance. The relative bias $b_{\hat{\theta}}$ of the estimator $\hat{\theta}$ of the parameter θ is defined as $b_{\hat{\theta}}=E|\hat{\theta}-\theta|/\theta$, and the relative variance is $v_{\hat{\theta}}=E(\hat{\theta}-\theta)^2/\theta^2$, where E is the mathematical expectation.

Table 1: Performance of the ARCAP (AC), ARAPES (AA), filterbank implementation of the ARCAP (FB-AC) and ARAPES (FB-AA) and frequency shifted filter bank implementation of the ARCAP (FBS-AC) and ARAPES (FBS-AA) methods.

	AC	AA	FB-AC	FB-AA	FBS-AC	FBS-AA
Relative bias of frequency estimations						
0dB	2.10^{-4}	2.10^{-4}	3.10^{-3}	2.10^{-3}	10^{-4}	10^{-4}
6dB	2.10^{-5}	2.10^{-5}	2.10^{-3}	10^{-3}	10^{-4}	10^{-5}
Relative variance of frequency estimations						
0dB	10^{-4}	10^{-4}	4.10^{-3}	6.10^{-4}	10^{-3}	10^{-3}
6dB	3.10^{-6}	3.10^{-6}	3.10^{-4}	10^{-4}	10^{-4}	10^{-4}
Relative bias of amplitude estimations						
0dB	6.10^{-2}	10^{-2}	6.10^{-1}	4.10^{-2}	4.10^{-1}	9.10^{-2}
6dB	7.10^{-2}	2.10^{-3}	7.10^{-1}	10^{-1}	6.10^{-1}	2.10^{-1}
Relative variance of amplitude estimations						
0dB	10^{-2}	10^{-2}	8.10^{-2}	3.10^{-2}	8.10^{-2}	5.10^{-2}
6dB	6.10^{-3}	3.10^{-3}	6.10^{-2}	4.10^{-2}	8.10^{-2}	7.10^{-2}

It is readily observed that the ARAPES amplitude estimator outperforms the ARCAP method both in bias and variance. The frequency estimator exhibits the same performance since the AR step is performed on the same data.

The performances of the estimators are dramatically degraded when the methods are implemented within the filterbank framework (FB-AC and FB-AA). This can be partly explained by the frequency shift due to the centre frequency of the computed filters as pointed out on Figure 5.

As a matter of fact when performing the frequency-shift procedure before the filterbank analysis one can observe the reduction of the bias and variance of the frequency estimator. However the ARCAP and ARAPES methods still perform better.

The amplitude estimation is still an issue. The theory of Rao and Pearlman⁽¹⁴⁾ states that the filterbank implementation of the AR spectral estimation method performs better than its full-band equivalent provided ideal filters. In practice filters are required to be band-limited and such that the bandpass do not overlap. Figure 5 clearly shows that the Capon and APES filters are not band-limited. Side lobe effects make this implementation highly unstable since as already pointed out that a bias in the frequency estimation may lead to a dramatic behaviour of the amplitude estimator.

6. Diagnosis of rail corrugation

The ARAPES method has been applied to the analysis of a corrugation measurement. The signal was recorded on a 20m long section of rail of the line B of the French RER network. The sampling rate was $T_s=4\text{mm}$, so the data length is $N_x=5000$ samples. The ARAPES method was applied on 2m long signal segment, that is $N=500$ samples and the model order was $p=200$. The computed ARAPES map is displayed on Figure 6 along with the analysed signal and the Welch periodogram computed on a rectangular window of size N . The mileage resolutions of the Welch periodogram and the ARAPES are thus equal.

Assuming a critical mode depth of 30mm for refurbishment to be performed, a 30mm threshold has been applied to the ARAPES map. All the estimated components with amplitude lower than this threshold have thus been removed. The amplitudes are displayed on a colour scale in mm.

The corrugation amplitudes are not constant with the mileage and critical corrugation level has been detected on 4 sections of rail by the ARAPES method has detected. Diagnosis based on the Welch periodogram only, as recommended by European standard⁽⁶⁾, is not able to provide this mileage information. The further computation of the rms of the recorded signal as required by European standard⁽⁵⁾ would be mandatory. Diagnosis based on the Welch periodogram only would have thus conclude to the need of rail refurbishment although it is observed from the ARAPES map that the longest critical corrugation section is about 4m long. It is too short to produce disturbances.

Note also that the 4 corrugation patterns do not bear the same wavelengths. The two last patterns exhibit components in the 12.5-25cm wavelength band. Again the observation of the Welch periodogram does not give access to this information. Eventually note that the Welch periodogram exhibits only one spectral peak in the 50-100cm wavelength band whereas two modes have been detected by the ARAPES method. This illustrates the better resolution power of the ARAPES method over the Welch periodogram.

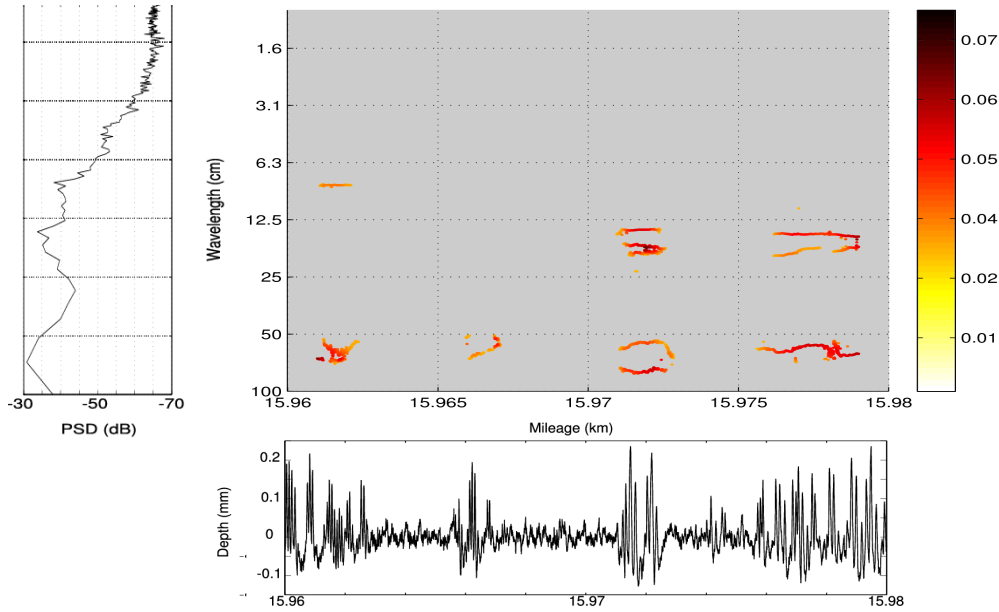


Figure 6: ARAPES(200) map of a corrugation recording thresholded at 0.03mm. The amplitudes are expressed on the color scale in mm.

7. Conclusions

The diagnosis of rail corrugation is an issue for railway network operators since it produces noise-disturbance and reduces the lifetime of the involved structures. So far, and as recommended by European standards, the monitoring of railway corrugation is performed either in the mileage or wavelength domain, implicitly assuming stationarity of the corrugation modes. We have proposed to apply the ARCAP method for the diagnosis of rail corrugation. This high-resolution method allows for a wavelength tracking of the modes but it suffers from relatively poor performances. We have thus proposed some modification of the algorithm in order to increase the capability of the amplitude and frequency estimations. Experimental results show that the use of the APES method for amplitude estimation in place of the Capon method allows for reduced bias and variance. We have also proposed to implement the method in a filterbank framework in order to increase the wavelength estimation performance since the formulation of the APES (and Capon as well) method is based on the derivation of a matched filterbank.

However observations show that the derived filterbank is not band-limited. This is mandatory for a filterbank implementation. We are currently working on improving the filter design in the matched filterbank estimation of the amplitude.

Acknowledgements

The authors would like to thank Dr. Nadine Martin for valuable comments about the behaviour of the Capon filter impulse response.

References and footnotes

1. Y. Sato, A. Matsumoto and K. Knothe, 'Review on rail corrugation studies', *Wear*, Vol 253, pp 130-139, 2002.
2. S. L. Grassie and J. Kalousek, 'corrugation: characteristics, causes and treatments', *Proceedings Inst. Mech. Eng*, Vol 207-F, pp 57-68, 1993.
3. S. L. Grassie, 'Rail corrugation: advances in measurement, understanding and treatment', *Wear*, Vol 258, pp 1224-1234, 2005.
4. J. Kalousek and S. L. Grassie, 'Rail corrugation: causes and cures', *International Railway Journal*, 24-26, July 2000.
5. European standard prEN 13231-3. 'Railway applications – Track – Acceptance of works – Part 3: Acceptance of rail grinding, milling and planing work in track'.
6. European standard PrEN 15610. 'Railway applications – Noise emission – Rail roughness measurement related to rolling noise generation'.
7. P. Flandrin, 'Time-Frequency/Time-Scale Analysis'. Academic Press, 1999.
8. A. Caprioli, A. Cigada and D. Raveglia. 'Rail inspection in track maintenance: A benchmark between the wavelet approach and the more conventional Fourier analysis'. *Mechanical Systems and Signal Processing*. Vol 21, pp 631-652, 2007.
9. L. Padovese, N. Martin, and J.-M. Terriez. 'Temps-fréquence pour l'identification des caractéristiques dynamiques d'un pylône de téléphérique'. *Traitement du Signal*, Vol 13, No 3, pp 209-223, 1996.
10. S. L. Marple. 'Digital Signal Analysis with Applications'. Prentice-Hall 1987.
11. J. Capon. 'High-Resolution Frequency-Wavenumber Spectrum Analysis'. *Proceedings of the IEEE*. Vol 57, No 8, pp 1408-1418, August 1969.
12. H. Li, J. Li and P. Stoica. 'Performance Analysis of Forward-Backward Matched-Filterbank Spectral Estimators'. *IEEE trans. On signal proc.* Vol 46, No 7, July 1998.
13. J. Li and P. Stoica. 'An Adaptive Filtering Approach to Spectral Estimation and SAR Imaging'. *IEEE trans. On signal proc.* Vol 44, No 6, June 1996.
14. S. Rao and W. A. Pearlman. 'Analysis of Linear Prediction, Coding, and Spectral Estimation from Subbands'. *IEEE trans. On info. theory*. Vol 42, No 4, July 1996.
15. A. Tkacenko and P. P Vaidyanathan. 'Sinusoidal frequency estimation using filter banks'. *Proceedings of ICASP01*, Vol 5, pp 3089-3092, May 2001.
16. D. Levy. 'Conception d'un système de mesure et d'analyse de l'usure ondulatoire des rails'. *Revue générale des chemins de fer*, 108th year, pp 51-57, May 1989.
17. In expression (3) and throughout the rest of this paper the sampling frequency is set to unity in order to simplify mathematical writings.
18. P. Stoica, A. Jakobsson and J. Li. 'Matched-filter bank interpretation of some spectral estimators'. *Signal Processing*, Vol 66, No 1, pp 45-59, April 1998.
19. M. Durnerin and N. Martin. 'Minimum variance filters and mixed spectrum estimation'. *Signal Processing*, Vol 80, No 12, pp 2597-2608, December 2000.